2019

A novel solar-driven direct contact membrane-based water desalination system

Abdellah Sharifian
Edith Cowan University

Mehdi Khiadani
Edith Cowan University

10.1016/j.enconman.2019.112055
Shafieian, A., & Khiadani, M. (2019). A novel solar-driven direct contact membrane-based water desalination system. *Energy Conversion and Management*, *199*, Article 112055. Available here

This paper has been published as: Shafieian, A., & Khiadani, M. (2019). A novel solar-driven direct contact membrane-based water desalination system. *Energy Conversion and Management, 199*, 112055. doi:10.1016/j.enconman.2019.112055

A novel solar-driven direct contact membrane-based water desalination system

Abdellah Shafieian, PhD Candidate, School of Engineering, Edith Cowan University, 270 Joondalup Drive, Joondalup, Perth, WA 6027, Australia

Email: a.shafieiandastjerdi@ecu.edu.au

Mehdi Khiadani, Associate Professor, School of Engineering, Edith Cowan University, 270 Joondalup Drive, Joondalup, Perth, WA 6027, Australia.

Tel.: +61 8 6304 5825; fax: +61 8 6304 5811.

Email: m.khiadani@ecu.edu.au (author for correspondence)

Abstract

This study proposes a novel integrated solar membrane-based desalination system. The system includes vacuum glass tubes to increase absorbed solar energy and to decrease heat loss, heat pipes to transfer the absorbed energy efficiently, and a tubular direct contact membrane distillation module to use the absorbed energy more effectively. To improve the freshwater production rate and overall efficiency of the proposed system, a cooling unit was also added to the permeate loop of the desalination unit. The performance of the system was experimentally investigated without (Case I) and with (Case II) the cooling unit in summer and without the cooling unit in winter (Case III) under climatic conditions of Perth, Western Australia. The experimental results indicated that except a few minutes in the morning, the heat pipe solar system was able to provide all the required thermal energy for the desalination system. The maximum thermal efficiency of the solar system in summer reached ~78% and its exergy efficiency fluctuated between 4-5% for a noticeable amount of time from 10:30 AM to 3 PM. Moreover, the maximum freshwater production rate were 2.78, 3.81, and 2.1 L/m^2h in Cases I, II, and III, respectively. The overall efficiency of the system improved from 46.6% in Case I to 61.8% in Case II showing the technical effectiveness of implementing the cooling unit in the permeate flow loop of the system. In addition, the daily averaged specific energy consumption in Cases I, II, and III were 407, 377, and 450 kWh/m^3, respectively.

Keywords: Solar desalination; Direct contact membrane distillation; Freshwater production; Heat pipe

Nomenclature

A_c	Collector area (m^2)	n	Number of error sources
C_f	Heat capacity of saline feed stream (kJ/kgK)	s	Specific entropy (kJ/kgK)
C_{wf}	Heat capacity of the solar working fluid (kJ/kgK)	T_0	Temperature at dead state (K)
dest	Destroyed	T_{sr}	Solar radiation temperature (K)
dist	Distilled	$T_{wf,i}$	Collector inlet temperature (°C)
$\dot{E}x$	Exergy (kW)	$T_{wf,o}$	Collector outlet temperature (°C)
$\dot{E}x_u$	Useful exergy (kW)	out	Outlet
$\dot{E}x_{sc}$	Absorbed exergy by solar collector (kW)	p	Permeate/Pump
f	Feed	$\dot{Q}$	Heat transfer rate (kW)
G	Solar radiation intensity (kW/m^2)	$\dot{Q}_{ab}$	Transferred energy to the solar working fluid (kW)
GOR	Gained output ratio	$\dot{W}$	work rate (kW)
H	Heater	W_R	uncertainty of the calculated parameters
h	Specific enthalpy (kJ/kg)	W_t	total uncertainty
h_{fg}	Latent heat of evaporation (kJ/kg.K)	w	Water
in	Inlet	**Greek letters**	
J	Mass flux (kg/m^2s)	φ	Physical exergy flow (kJ/kg)
m	Membrane	ε_s,	Systematic errors
$\dot{m}$	Mass flow rate (kg/s)	ε_r	Random errors
$\dot{m}_{DCMD}$	Mass flow rate through the membrane (kg/s)	η_c	Thermal efficiency of HPSC (%)
$\dot{m}_f$	Mass flow rate of feed stream (kg/s)	η_{sc}	Exergy efficiency of HPSC (%)
$\dot{m}_{wf}$	Solar working fluid mass flow rate (kg/s)		

1. Introduction

Water shortage has affected millions of people around the world and predictions made by the World Health Organization evaluate the situation in the future as a warning [1]. The almost constant amount of potable water on earth, rapid population growth, and increasing food demand have put significant stress on the available potable water sources [2]. For instance, the average water consumption of Perth residences in Western Australia was 155-166 L/day per person in the period of 1998-2001 [3] which has increased to 337 L/day per person in 2017-18 [4]. Meanwhile, the annual average rainfall has decreased by 3mm/year and the annual mean temperature has increased by 1℃ [4].

Many researchers have tried to combat the global issue of severe water shortage by proposing various desalination methods aiming to produce freshwater from seawater. However, the proposed methods demand considerable amounts of energy and parameters such as high energy cost and consequent environmental problems have affected their technical and economic feasibility negatively. This has acted as a great motivation for researchers to implement solar energy as a clean and renewable energy source in desalination techniques.

Various solar desalination systems including solar stills [5], reverse osmosis [6], humidification dehumidification [7], and multi-stage desalination [8] have been studied; however, different practical and economic complications such as low freshwater productivity, low water quality, fouling generation, polarization films formation, and most importantly high energy demand have restricted their application [9]. In recent years, a promising newcomer to the desalination methods called direct contact membrane distillation (DCMD) has gained attractions due to its unique features and noticeable advantages.

Membrane-based desalination technique requires less pre-treatment [10], has low heat loss, operates with low pressures, has simple operation and higher efficiencies, and requires the least

equipment [9]. In addition, the driving force across the membrane can be provided by even moderate temperatures enabling the integration of DCMD units with solar systems [11]. Moreover, the salinity of the seawater does not affect the performance of DCMD units [10]. The DCMD is the oldest and most widely used process having low initial and maintenance cost. In addition, its high-efficient performance has been well studied and proven resulting in the more technical and economic feasibility of the desalination system in which this process is used. However, several challenges have hampered the progress of membrane distillation in industrial stage. The main challenges which need to be resolved are limited flow dynamics [12], fluctuations in capital costs of investment [13], and fouling issues resulting in lower overall efficiency [9].

Membrane module includes two channels for hot (feed) and cold (permeate) flow streams which are separated by a membrane module having a specific porosity. Water molecules evaporate from saline water and transfer from the feed stream having higher vapour pressure to the permeate stream having a lower vapour pressure [14]. Regarding energy consumption and water production cost range, different and even conflicting results have been reported ranging from 1 kWh/m^3 to 9,000 kWh/m^3 [13]. These parameters depend greatly on laboratory system, configuration, and operational conditions. However, it has been proved that more than 90% of this energy can be provided by solar energy [9].

To date, several researchers have tried to propose innovative designs for a combination of solar energy and DCMD modules. Bouguecha et al. [15] used flat plate solar collectors to drive a solar DCMD system. Shim et al. [16] developed a novel unsteady mathematical model to estimate the freshwater production rate of a flat plate solar DCMD system. In a theoretical study, Ma et al. [17] used simultaneous mass and heat transfer equations to study the connection of a flat plate solar system to a DCMD module for small-scale units in remote areas.

Another type of solar collectors that have been widely used in solar systems is evacuated, tube collector. This collector is made of parallel evacuated glass pipes and has significant advantages compared to the flat plate collectors [18]. Elzahaby et al. [10] integrated an evacuated tube solar system with a DCMD unit and evaluated the sensitivity of the system to several parameters such as salt concentration, feed flow rate, and membrane physical characteristics.

A similar experimental study was conducted by Kabeel et al. [19] in which the performance of the solar system was investigated under actual climatic conditions. Chafidz et al. [20] combined evacuated tube solar thermal collectors, flat plate solar photovoltaics, and membrane distillation units to create a self-contained solar desalination system suitable for operation in arid remote areas.

Another configuration which has attracted several researchers in recent years is the combination of solar ponds and membranes. Suarez et al. [21] experimentally investigated the performance of a DCMD unit driven by solar ponds. In a similar study, Nakoa et al. [2] connected a DCMD unit directly to a solar pond and analyzed its performance throughout a day both theoretically and experimentally. Rahaoui et al. [22] investigated the performance of a DCMD unit in conjunction with a solar pond under high saline water with zero brine discharge. The result indicated that the feed temperature was the most important parameter of the system.

Kim et al. [23] proposed a solar membrane-based desalination system having novel energy recovery concepts. Chang et al. [24] proposed an automatic control function as a strategy to maximize the freshwater production rate of solar membrane-based desalination systems. Similar theoretical and experimental investigations have also been carried out to propose a solar-driven stand-alone desalination system for remote areas [25], to analyse the performance

of different types of membranes in solar systems [26], and to desalinate well water using solar-driven systems [27].

In a comprehensive review paper, Qtaishat and Banat [28] summarized various techniques to couple solar energy to a DCMD unit. Heat and mass processes of the membrane units were discussed in the paper and previously studied solar combinations including solar photovoltaic, solar thermal, and solar ponds, as well as solar collectors were discussed. In another review paper, Sharon and Reddy [29] summarized various membrane types integrated with solar systems. The performance of the previous proposed systems, their problems and restrictions, proposed novel methods, and economic issues have also been covered in their paper.

Despite many efforts and studies that have been carried out to date, integrating solar energy and membrane technology is not yet a straightforward matter and has many opportunities for technical and economic improvements. The drawbacks of conventional solar systems have negatively affected the feasibility of solar membrane-based desalination systems. Flat plate solar systems have high hydraulic resistances and limited heat transfer capacity [30], require sun trackers, and are vulnerable condensation and moisture [18]. Moreover, the possibility of water freezing exists during cold seasons and their thermal efficiency decreases significantly in hot seasons as the ambient temperature goes up and thermal losses increase [31].

Evacuated tube solar systems perform slightly better during cold seasons, however, the possibility of overheating still remains as an important drawback of these systems [32]. Besides, the solar working fluid flows inside the glass tubes which affect their performance negatively (e.g., glass break, freezing, and etc.) [33]. Direct contact between saline water and components of solar collector is another drawback of the proposed systems increasing the possibility of sedimentation, corrosion, and rustiness resulting in high maintenance cost and low efficiency. In addition, the main challenge of previous proposed solar desalination systems

is their low freshwater production rate. Freshwater productivity, which is the most important parameter in the development of solar desalination systems, still needs improvement.

To overcome the abovementioned disadvantages of solar desalination systems, a novel integrated system taking advantage of heat pipes, evacuated glass tubes, and DCMD technologies is presented in this paper for the first time. This system intends to improve the technical and economic feasibility of solar desalination systems by not only driving the desalination unit using a high-efficient solar system but also by providing an integrated system with high freshwater productivity. The proposed system was manufactured and tested experimentally in summer and winter under real climatic conditions of Perth, Western Australia. Moreover, in a separate scenario and with the aim of improving the performance of the proposed system, a cooling unit was added to the permeate loop of the desalination system. The technical effectiveness of implementing the cooling unit on freshwater production rate, gained output ratio, and overall efficiency of the system was investigated experimentally. It is often difficult and expensive to deliver water to remote areas and regional towns. The proposed system can work effectively as a stand-alone system in these areas. The system also has a great potential to be applied in large-scale and industrial applications or in desalination plants.

2. Experimental setup and instrumentation

Figures 1 and 2 show the overall schematic and real picture of the proposed heat pipe solar-driven direct contact membrane-based desalination system. The main aims of the new design were driving the desalination unit using a high-efficient solar system in terms of solar energy absorption and transition and applying the absorbed energy in an efficient manner using an integrated system with high freshwater productivity. The system consists of three main loops including the solar heating loop, membrane feed loop, and membrane permeate loop.

The main duty of the solar loop is converting solar energy into thermal energy and transferring this energy to the saline water inside the feed tank. Application of evacuated tubes and heat pipes in this loop not only decreased the heat loss but also resulted to an efficient heat transfer process. The hot saline water is pumped to the DCMD module (feed channel) through the membrane feed loop. At the same time, the cold permeate water is pumped to the permeate channel of the DCMD module (membrane permeate loop). The operational processes of these three loops along with their characteristics are explained in details in the following sections. A central control unit consisting of a power unit, a National Instrument Data Acquisition (NIDAQ) system, and a computer was used to collect data, monitor the experimental results, and control the operation of the system.

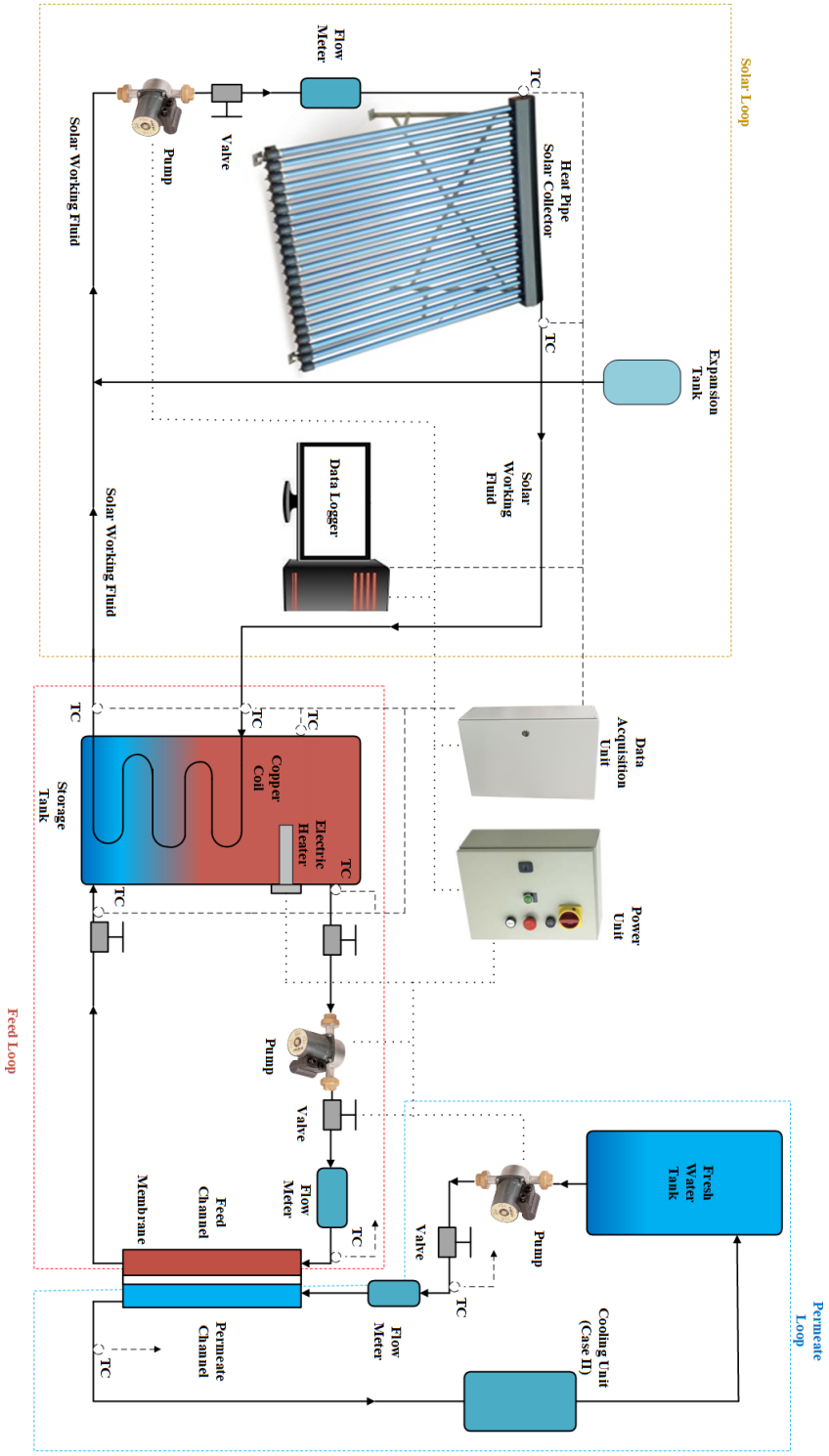

Fig. 1. Schematic of the heat pipe solar membrane-based desalination system

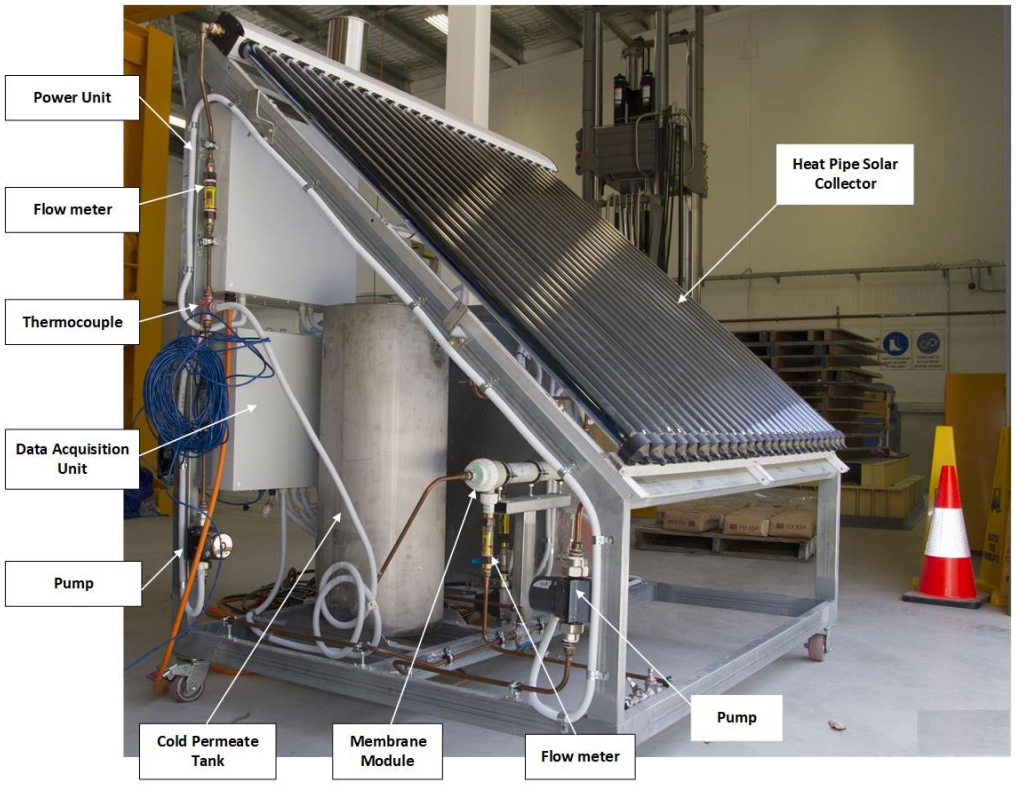

Fig. 2. The experimental rig manufactured and used in this study

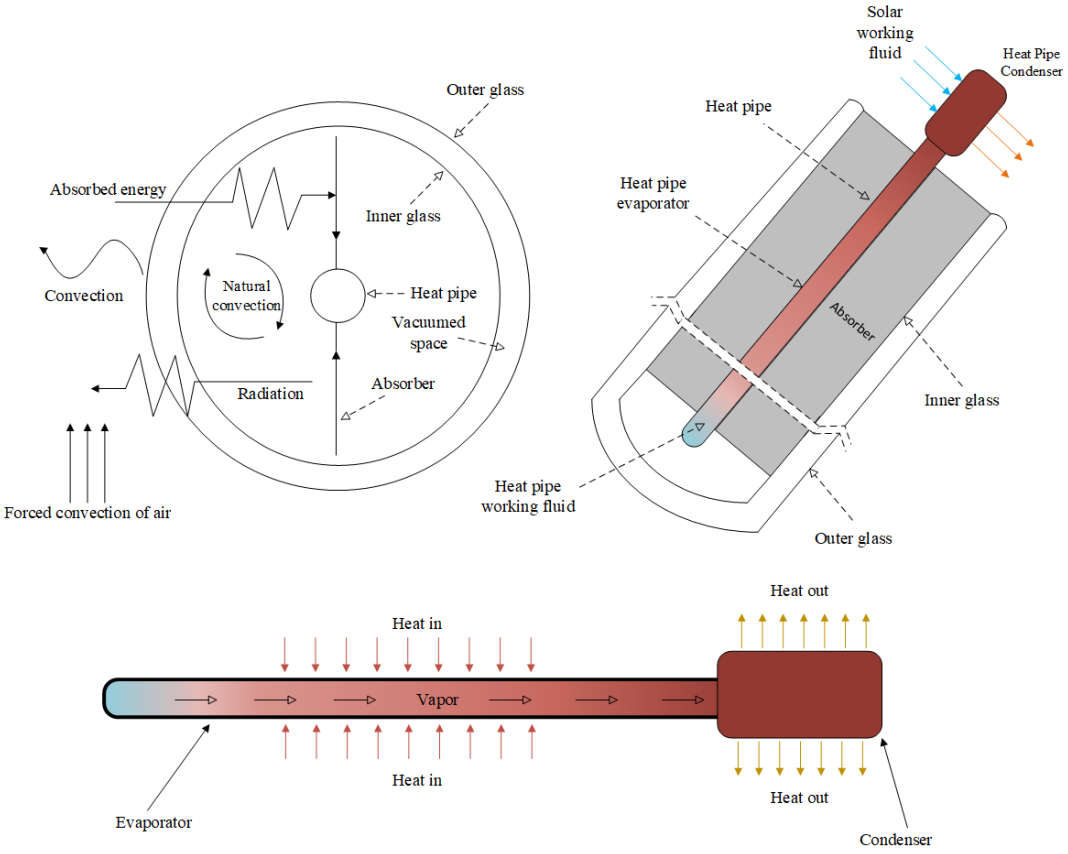

Fig. 3. Schematic of heat transfer processes inside a vacuum glass tube of a HPSC [34]

2.1. Solar heating system

The main component of the solar heating system is the heat pipe solar collector (HPSC) consisting of heat pipes and vacuum-sealed glass tubes (Fig. 3). Except minor dimensional distinctions, no significant difference has been observed in the thermal efficiency of almost all the commercial available HPSCs. The main influencing factors on the efficiency and amount of absorbed energy in these collectors are the solar working fluid, the inlet temperature of the collector, and climatic conditions. Therefore, based on the design and application, a HPSC made by Century Sun Energy Technology Company in China was purchased and its information was provided in Table 1.

Table 1. Components of heat pipe solar collector along with their specifications [35]

Solar collector		**Heat pipe**		**Vacuum Glass**	
Number of tubes	25	Material	Red copper	Emissivity	0.07
Gross area (m^2)	3.93	Condenser Length (m)	0.10	Transmittance	0.88
Manifold diameter (m)	0.038	Outer diameter (m)	0.008	Thickness (m)	1.60
Manifold material	Red copper			Outer diameter (m)	0.058
Insulation	Compressed Rockwool				
Tube length (m)	1.80				
Absorptivity	0.94				

A portion of the stroked solar radiation is absorbed and used to vaporize the heat pipe working fluid (i.e. methanol) while another portion is dissipated back into the environment [36]. The walls and wick structure of heat pipes are made of copper. The heat pipe working fluid in the form of vapour moves upwards and reaches the condenser section of heat pipes which are located inside a manifold. The manifold acts as a heat exchanger and the thermal energy is transferred from the heat pipe condensers to the solar working fluid flowing inside the manifold

using a pump. The heat pipe working fluid turns into a liquid state by exchanging thermal energy and returns to the evaporator section. At the same time, the temperature of the solar working fluid (i.e. distilled water) flowing inside the manifold increases as it moves along the manifold and over heat pipe condensers. The hot solar working fluid coming out of collector outlet enters the copper coil located inside the storage tank and transfers its heat to the saline water inside the tank.

The pump used to circulate the solar working fluid was made by Davey company and a valve was used to regulate its mass flow rate. The mass flow rate of the solar working fluid was set at the constant value of 3 L/min. A FL-9200 flowmeter made by Omega company was utilized to monitor the solar working fluid mass flow rate. The capacity of the saline water storage tank was 210 L and was insulated by 50-mm thermal insulation layers. The length and external heat transfer area of the copper coil inside the feed tank was, 34 m and 1.45 m^2, respectively. A 2 kW auxiliary heater was also installed inside the feed tank to be operated when solar radiation is not enough to supply all the required thermal energy for the desalination system.

2.2. Direct contact membrane distillation

A DCMD module comprises two channels (i.e. feed (hot) and permeate (cold) channels), separated by a porous membrane (Fig. 4a). Due to the higher temperature of the saline feed stream compared to the permeate stream, the vapour pressure in the feed channel is higher than the permeate channel. Water molecules near the hot surface of the membrane evaporate from the saline stream and move towards the cold surface while the vapour pressure difference acts as the main driving force for this mass flux through the membrane. The required thermal energy for evaporation is provided by the hot feed stream flowing in the feed channel. On the other surface of the membrane, the vapour molecules condense to liquid transferring the condensation thermal energy to the cold permeate stream flowing in the permeate channel [14].

A tubular membrane made by Enka-Microdynn company was used in this study (Fig. 4b). The membrane module consisted of 19 feed channels covered in a shell that has 4 inlet and outlet ports (Fig. 4b). The specifications of the tubular direct contact membrane distillation module are presented in Table 2.

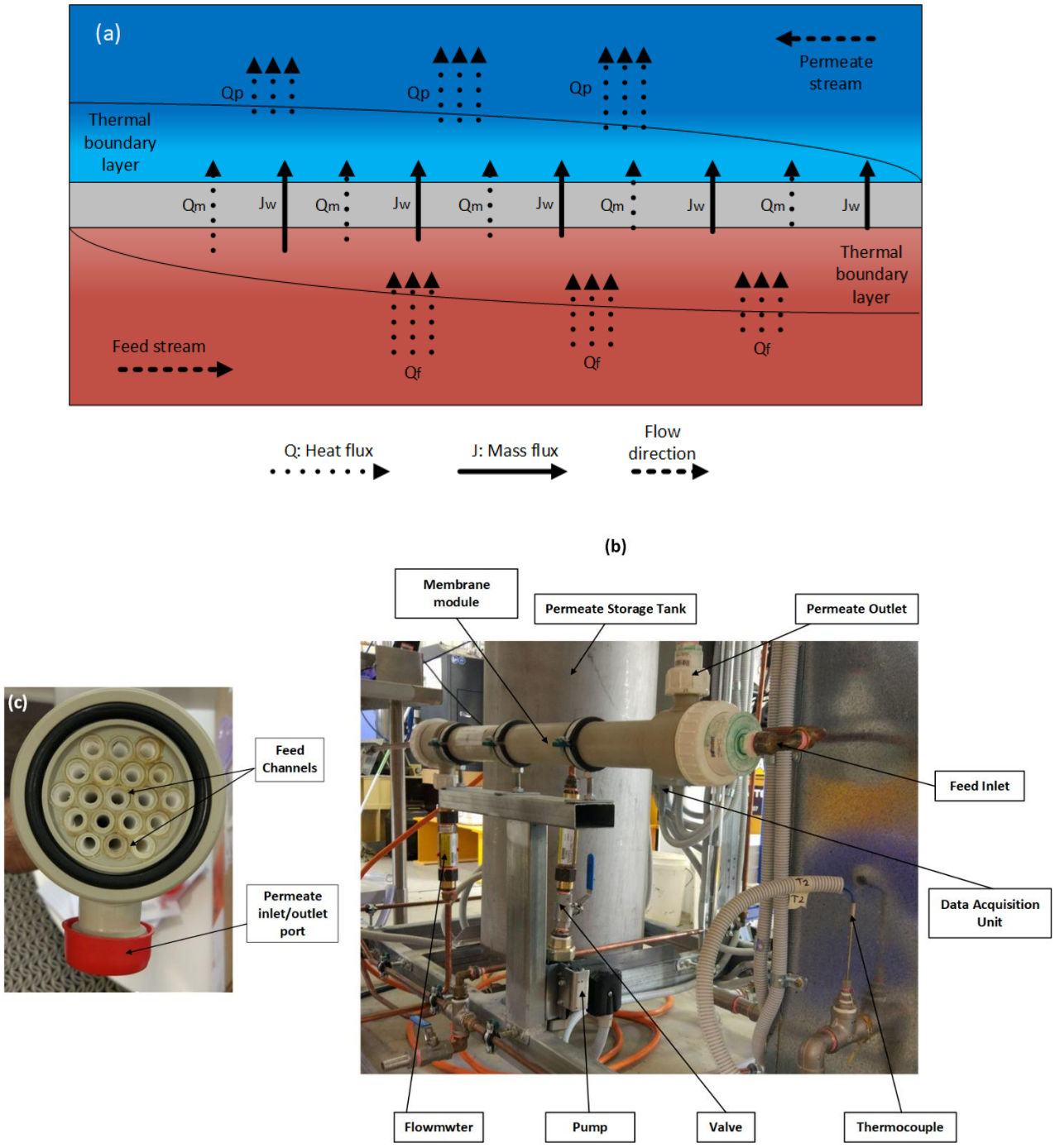

Fig. 4. (a) Schematic diagram of heat transfer process in DCMD modules, (b) components of the tubular DCMD setup, and (c) cross section of the membrane.

Table 2. The specifications of the tubular direct contact membrane distillation module [37]

Characteristic	**Value**	**Characteristic**	**Value**
Model type	MD 090 TP 2N ANSI	Membrane material	Polypropylene
Membrane module length	75 cm	Potting material	Polypropylene
Membrane area	0.2 m^2	Outer diameter of membrane module	8.5 mm
Nominal module diameter	9 cm	Outer shell material	Polypropylene
Inner diameter of membrane module	5.5 mm	Membrane thickness	1.5 mm
Average pore size	0.2 µm	Membrane porosity	75%

To make the synthetic seawater (salinity of 3.5%), Sodium Chloride made by Chem-supply Company was dissolved in tap water and the salinity of the storage tank was monitored using a conductivity meter type Multi 3410 made by WTW company. A pump made by Davey Company was used to extract saline water from the storage tank and circulate it in the feed loop of the desalination system and its flow rate was regulated via a valve installed after the pump. The FL-9000 EZ flowmeter made by OMEGA company was used to monitor the saline water mass flow rate (Fig. 4b). The same equipment was used for the permeate loop of the desalination system. The cold freshwater was extracted from the permeate tank and circulated in the permeate channel of the membrane module.

2.3. Experimental procedure

The conducted experiments followed two aims, one to investigate the performance of the novel integrated heat pipe solar membrane-based desalination system throughout a day under real climatic conditions in summer and winter (Cases I and III), and the other to evaluate the effectiveness of adding a cooling unit to the permeate loop and decreasing the permeate flow temperature in summer on improving the freshwater production rate and consequently the overall efficiency of the solar desalination system (Cases I and II). The idea behind the second aim is that in summer, the temperature of the permeate flow increases significantly by the passage of time and continuous heat transfer between hot and cold channel, which in return decreases the temperature difference between two surfaces of the membrane resulting in lower vapour pressure difference and mass flux through the membrane.

It is worth noting that temperature at various points of the system was measured using T- Class type thermocouples made by TC Ltd. which were all connected to the National Instrument Data Acquisition system. An application program interface was written in LabVIEW 2014 software to record data at 10-second intervals.

2.4. Climatic conditions

The system was operated under conditions of Cases I and II on 16 and 17 January 2019, respectively. These two days had similar climatic conditions and provide a reliable basis to compare two cases with each other. As these two days represent the summer days in the southern hemisphere, several experiments were also conducted in winter days and the results of 7 June 2019 was chosen to be presented in this paper as Case III.

Figure 5a shows the solar radiation in summer and winter days while Fig. 5b depicts the ambient temperature of the same days. The solar radiation intensity was almost similar at all times of two days. The ambient temperature in two days was also close to each other with few

degrees of divergence at specific times of the day. Taking this fact into account that the influence of solar radiation intensity on the thermal performance of heat pipe solar systems is more significant than ambient temperature [34], one can claim that two experiments have been performed in almost similar climatic conditions.

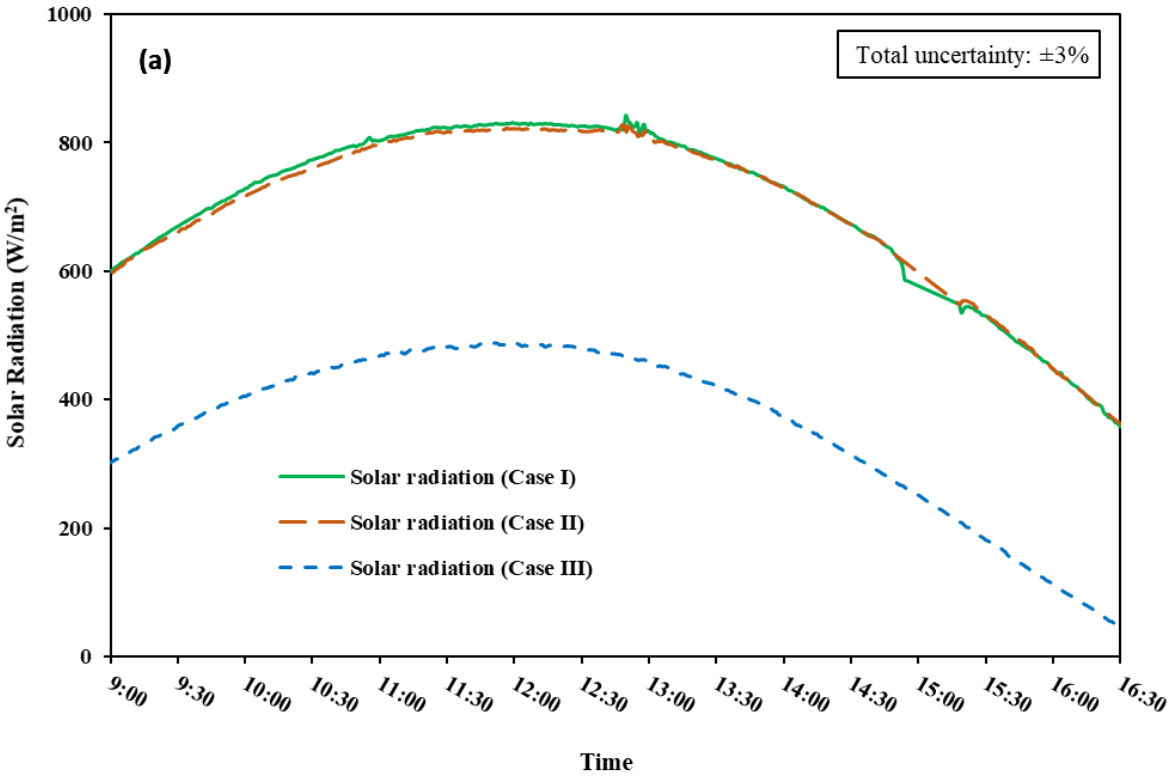

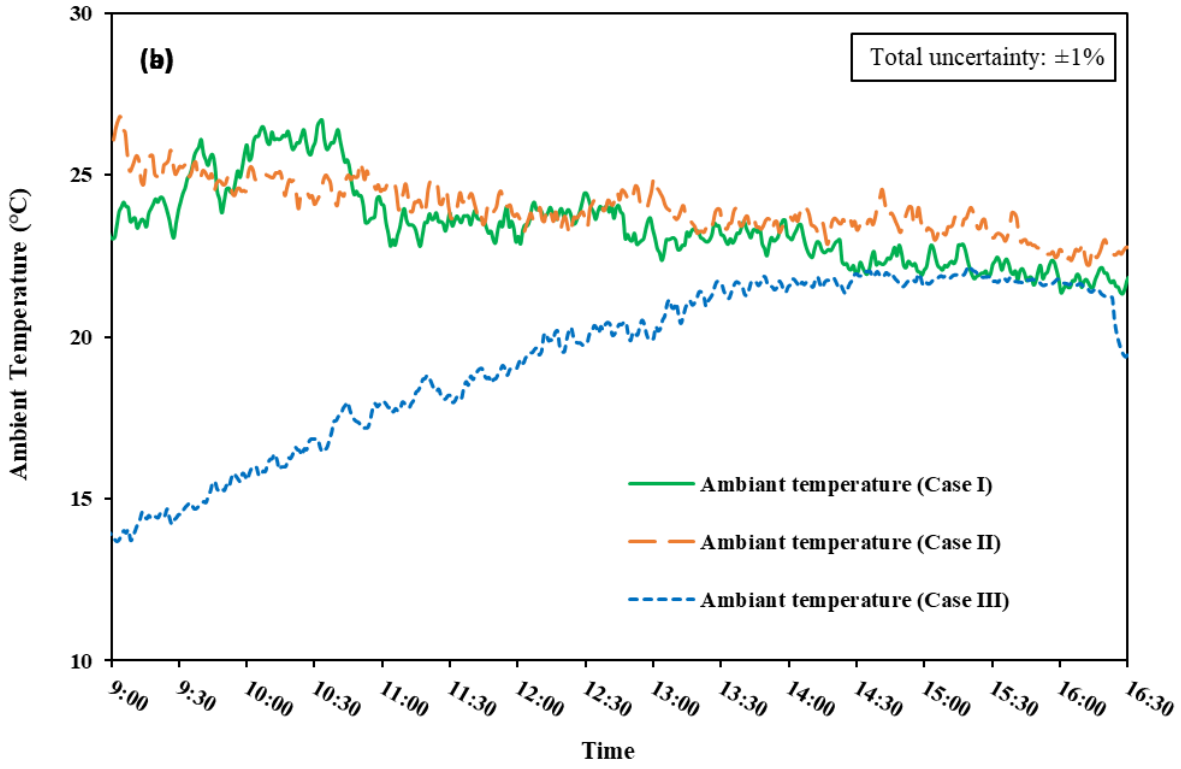

Fig. 5. Climatic conditions under which the experiments have been conducted: (a) solar radiation and (b) ambient temperature

3. Governing equations

3.1. Energy and exergy efficiency

The amount of transferred energy to the solar working fluid can be determined by [38]:

$$\dot{Q}_{ab} = \dot{m}_{wf} C_{wf} (T_{wf,o} - T_{wf,i}) \quad (1)$$

where $T_{wf,i}$ (°C) and $T_{wf,o}$ (°C) are inlet and outlet temperatures of the solar collector, respectively. In this equation, $\dot{m}_{wf}$ (kg/s) and C_{wf} (kJ/kgK) also represent the mass flow rate and heat capacity of the solar working fluid. The heat capacity was considered constant as the range of its changes is negligible in the range of solar working fluid temperature changes.

The thermal efficiency of the HPSC (η_c) can be obtained from [39]:

$$\eta_c = \frac{\dot{Q}_{ab}}{G A_c} \quad (2)$$

where G (kW/m^2) and A_c (m^2) represent solar radiation and area, respectively.

Besides thermal analysis, exergy analysis is a useful tool to investigate the significant energy losses in terms of time and magnitude. It is also useful to study the opportunities for thermodynamic enhancement of the solar system by determining the parameters affecting the system's thermodynamic imperfection and evaluating them quantitatively resulting in more efficient design of solar systems [40].

The exergy balance equation of the system can be written as [41]:

$$\sum \dot{E}x_{in} - \sum \dot{E}x_{out} = \dot{E}x_{dest} \tag{3}$$

which can be expanded to the following equation [42]:

$$\sum \left(1 - \frac{T_o}{T_k}\right) \dot{Q}_k - \dot{W} + \sum \dot{m}_{in}\varphi_{in} - \sum \dot{m}_{out}\varphi_{out} = \dot{E}x_{dest} \tag{4}$$

where $\dot{Q}$ (kW) and $\dot{W}$ (kW) represent heat transfer and work rate, respectively, and φ (kJ/kg), is the physical exergy flow which can be determine by [43]:

$$\varphi_{in/out} = \left(h_{in/out} - h_0\right) - T_0(s_{in/out} - s_0) \tag{5}$$

where *h* (kJ/kg) and *s* (kJ/kgK) represent specific enthalpy and entropy, respectively. T_0 (K) is the temperature at the dead state and subscripts 'in' and 'out' stand for inlet and outlet, respectively. The exergy efficiency of the solar collector can be written as [44]:

$$\eta_{sc} = \frac{\dot{E}x_u}{\dot{E}x_{sc}} \tag{6}$$

where $\dot{E}x_u$ (kW) and $\dot{E}x_{sc}$ (kW) are the useful delivered and the collector absorbed exergy, respectively, and can be determined by [40]:

$$\dot{E}x_u = \dot{m}_{wf}[(h - h_0) - T_0(s - s_0)] \tag{7}$$

$$\dot{E}x_u = \dot{m}_{wf}C_{wf}[(T_o - T_i) - T_0\left(\ln\frac{T_o}{T_i}\right)] \tag{8}$$

$$\dot{E}x_{sc} = AG\left[1 + \frac{1}{3}(\frac{T_o}{T_{sr}})^4 - \frac{4}{3}(\frac{T_o}{T_{sr}})\right] \tag{9}$$

where T_{sr} (K) represents the solar radiation temperature and its quantitative value is 6000 K.

The overall exergy efficiency of the solar system (η_s) can be defined as the useful delivered exergy to the storage tank ($\dot{E}x_{u,st}$) divided by the collector absorbed exergy ($\dot{E}x_{sc}$) [45]:

$$\eta_s = \frac{\dot{E}x_{u,st}}{\dot{E}x_{sc}} \tag{10}$$

Equations to calculate the useful delivered exergy to the storage tank and the exergy efficiency of other components of the solar system can be found in [40, 45].

To investigate the performance of desalination processes, a parameter called gained output ratio (GOR) is used which quantitatively represents the effectiveness of water production and is defined mathematically as [2]:

$$GOR = \frac{\dot{m}_{DCMD} h_{fg}}{\dot{m}_f C_f (T_{f,o} - T_{f,i})} \tag{11}$$

where $\dot{m}_{DCMD}$ (kg/s) and h_{fg} (kJ/kg.K) are mass flow rate through the membrane and latent heat of evaporation, respectively. Moreover, $T_{f,i}$ (°C) and $T_{f,o}$ (°C) are inlet and outlet temperatures of the saline feed stream, respectively. In this equation, $\dot{m}_f$ (kg/s) and C_f (kJ/kgK) also represent the mass flow rate and heat capacity of the saline feed stream.

The overall efficiency of the system is defined as the ratio of distilled water latent heat of vaporization to the total input energy rate of the system [10]:

$$\eta = \frac{\dot{m}_{DCMD} h_{fg}}{GA + \dot{W}_{p1} + \dot{W}_{p2} + \dot{W}_{p3} + \dot{W}_H} \tag{12}$$

where $\dot{W}$, *p, H* represent energy rate, pump, and heater, respectively.

The specific energy consumption, which is the combination of thermal and electrical energy consumption, is defined as the amount of energy required to produce a unit of fresh water. The specific energy consumption can be written mathematically as [9]:

$$EC = \frac{\dot{Q}_{heat} + \dot{W}_{p1} + \dot{W}_{p2} + \dot{W}_{p3} + \dot{W}_{H}}{\dot{m}_{dist}} \quad (13)$$

where $\dot{m}_{dist}$ (kg/s) is the flow rate of product and $\dot{Q}_{heat}$ (kW) is the total heat input rate and can be defined as [9]:

$$\dot{Q}_{heat} = \dot{m}_f C_f (T_{f,i} - T_{f,o}) \quad (14)$$

where $\dot{m}_f$ (kg/s) represents the feed inlet mass flow rate, C_{wf} (kJ/kgK) is the heat capacity of the feed fluid, and $T_{f,i}$ (°C) and $T_{f,o}$ (°C) are inlet and outlet temperatures of the membrane module, respectively.

3.2. Uncertainty analysis

Uncertainty analysis is a useful tool to determine the calculated and measured uncertainties. The measured parameters uncertainty consists of systematic errors, including data acquisition, calibration, and equipment accuracy, and random errors. The standard deviation method was applied to determine the total uncertainty [46].

$$W_t = \sqrt{{\varepsilon_s}^2 + {\varepsilon_r}^2} \quad (15)$$

where W_t, ε_s, and ε_r represent total uncertainty, systematic errors, and random errors, respectively. Following equations can be used to determine the systematic and random errors [46].

$$\varepsilon_s = \sqrt{\sum_{i=1}^{n} \varepsilon_{s,i}^2} \quad (16)$$

$$\varepsilon_r = \sqrt{\sum_{i=1}^{n} \varepsilon_{r,i}^2} \quad (17)$$

The parameter n in abovementioned equations represents the number of error sources and $\varepsilon_{r,i}$ can be determine by

$$\varepsilon_{r,i} = \sqrt{\frac{\sum_{i=1}^{n}(\varphi_i - \bar{\varphi})^2}{N(N-1)}} \quad (18)$$

where N represents the number of measurement repetitions and $\bar{\varphi}$ is the average value of the measurements.

Based on the propagation of errors method [3], the uncertainty of the calculated parameters (W_R) can be calculated from:

$$W_R = \sqrt{\sum_{i=1}^{n}\left(\frac{\partial R}{\partial x_i}W_i\right)^2} \quad (19)$$

where $R=R(a_1,a_2,\ldots,a_n)$, a_n is an independent variable and W is its uncertainty, respectively. Table 3 depicts the uncertainties of measured and calculated parameters in this study.

Table 3. Uncertainty analysis of measured and calculated parameters.

Parameter	**Instrument**	**Operation range**	**Systematic error (± %)**	**Random error (± %)**	**Total Uncertainty (± %)**
Temperature	Thermocouple	-185 – 300 °C	1.42	0.32	± 1.7
Flow rate	Flow meter	0 – 0.068 kg/s	1.34	0.45	±2
Ambient temperature	Air temperature sensor	-20 – 60 °C	1	0	±1
Wind velocity	Wind speed sensor	0 –75 m/s	2.6	0	±2.6
Solar radiation	Pyranometer	0 – 2000 W/m^2	3	0	±3
Thermal efficiency	-	-	-	-	±4.7
Exergy efficiency	-	-	-	-	±3.8

4. Results and discussions

4.1. Thermal analysis of the solar system

Figure 6 depicts the absorbed energy by the solar working fluid along with collector thermal efficiency as a function of time throughout the day. The lowest amount of absorbed energy (i.e. around 370, 250, and 120 W for cases I, II, and III, respectively) occurred at the beginning of the day because of low solar radiation. The amount of absorbed energy increased by the passage of time and reached the maximum value at around 10:30 AM for Cases I and II and around 11:00 AM for Case III . This was mainly due to the fact that solar radiation was high and at the same time the solar working fluid temperature was relatively low resulting in higher temperature difference between solar working fluid and heat pipe condensers and higher heat transfer rate inside the manifold section. The amount of absorbed energy started to decrease afterwards and reached 550 and 600 W for Cases I and II at the end of the day which was due to a gradual increase in collector inlet temperature. This can be observed in Fig. 7 which shows the collector inlet and outlet temperature in Cases I and II as a function of time throughout the day. The increase in solar radiation increased the collector outlet temperature and consequently increased the collector inlet temperature gradually in the closed-loop solar system. Higher values of collector inlet temperature led to lower heat transfer rate and absorbed energy by the solar working fluid.

The thermal efficiency of the HPSC almost followed the same trend as the absorbed energy. The thermal efficiency was around 35% at 9 AM and gradually increased by the passage of time. The thermal efficiency reached the maximum value of ~78% and started to decrease afterwards. This decrease was principally because of the increase in solar radiation, an increase in collector inlet temperature, and a decrease in the amount of absorbed energy. Consequently, the nominator in Eq. (2) decreased and denominator in this equation increased led to lower values of thermal efficiency. The thermal efficiency of the HPSC increased again in the

afternoon which can be explained by the fact that although the amount of absorbed energy decreased at those times, the solar radiation followed the same trend as well, resulting in lower values of the denominator in Eq. (2) and higher values of thermal efficiency.

The conclusion one can make from the results is that the difference between the thermal efficiency in two seasons was not significant; however, the amount of absorbed energy in summer was much higher resulting in higher collector outlet temperature and thermal capacity of the system. Therefore, to increase the thermal efficiency of the solar system in summer with its high solar radiation, the system should be operated at higher solar working fluid mass flow rates compared to winter. This increases both the thermal efficiency and thermal capacity of the solar heating system.

It can also be observed from the data in Fig. 7 that the collector inlet and outlet temperatures followed the same trend in both cases. However, the values of these parameters are lower in Case II compared to Case I. The reason for this behaviour is that using the cooling unit decreased the permeate flow temperature and at the same time increased the heat transfer between two surfaces of the membrane. Consequently, the temperature of the feed stream coming out of the membrane and returning to the feed tank decreased in Case II resulting in the lower average temperature of the feed tank. This in return increased the temperature difference between the solar working fluid flowing inside the copper coil and the saline water inside the feed tank, and as a result, the heat transfer increased and the solar working fluid coming out the copper coil (collector inlet) had lower values.

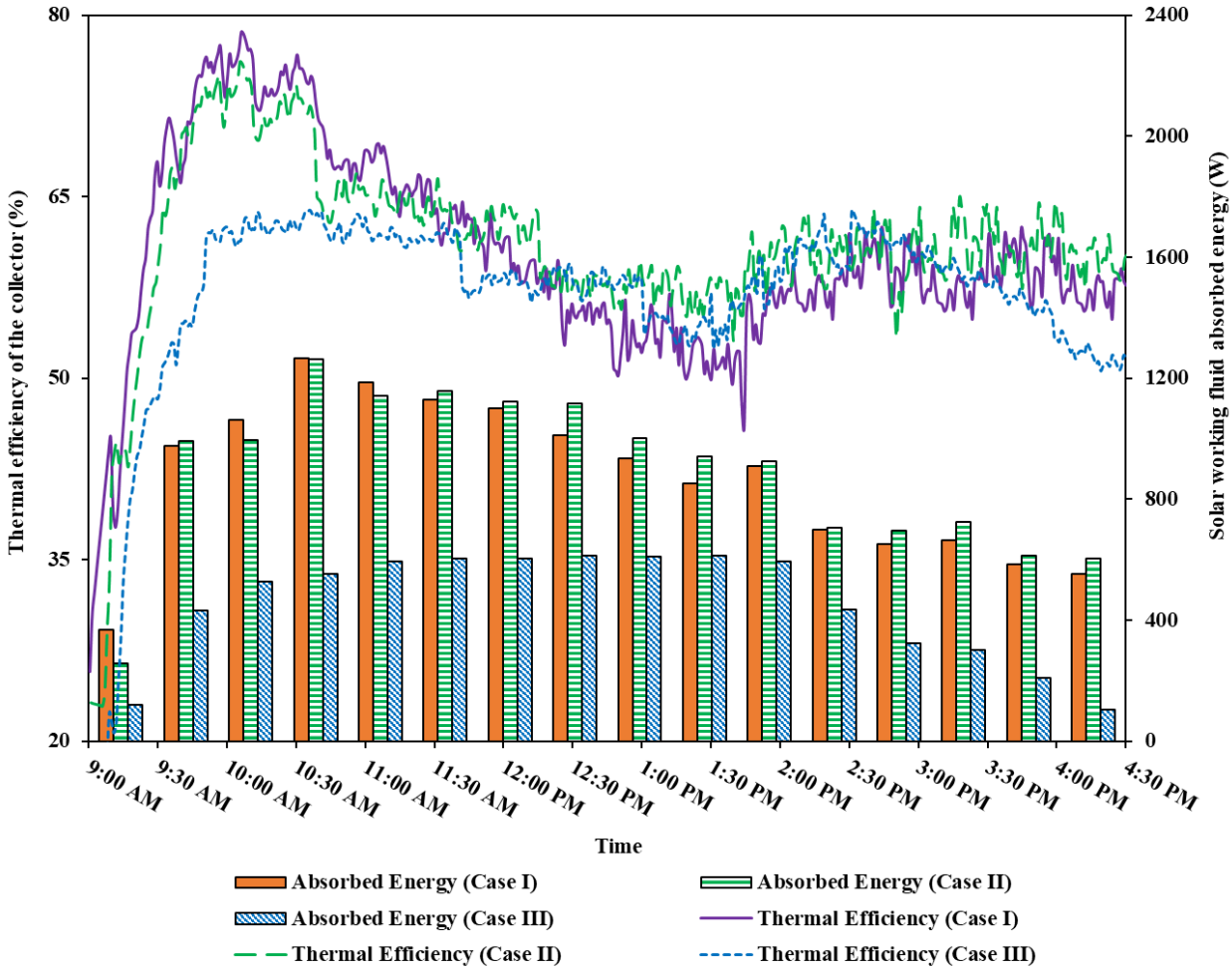

Fig. 6. Solar working fluid absorbed energy and thermal efficiency of the collector as a function of time

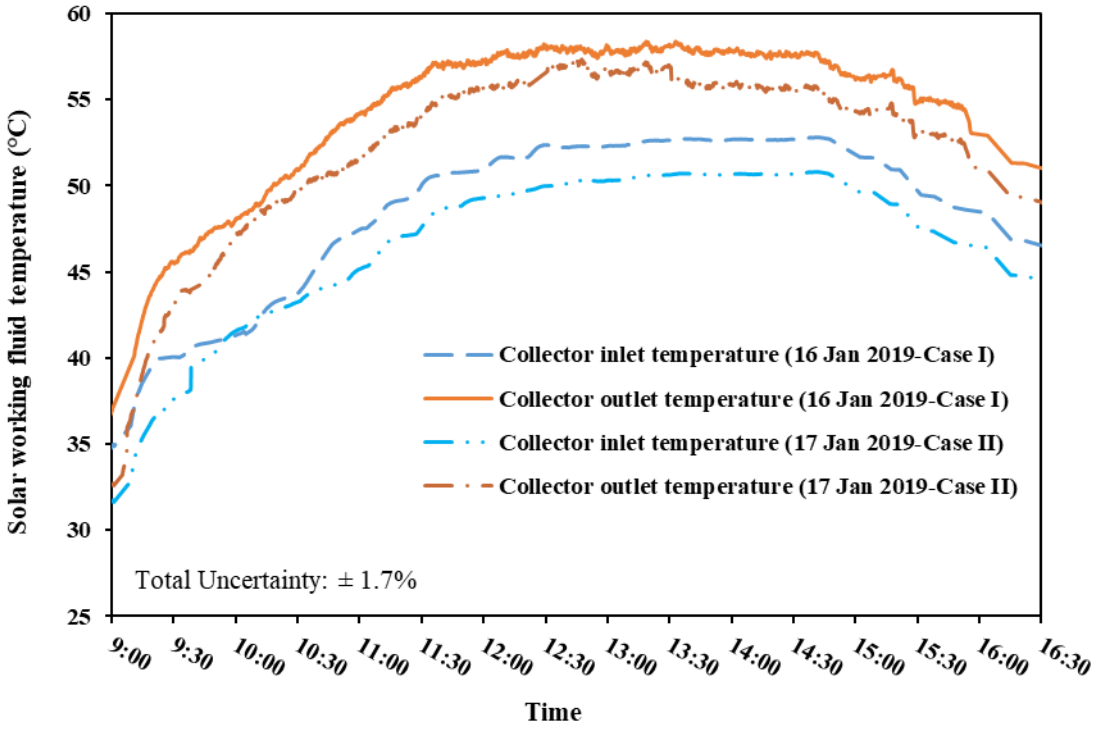

Fig. 7. Collector inlet and outlet temperature as a function of time in Cases I and II

Figure 8 indicates the exergy efficiency of the HPSC as a function of time in all cases throughout the day. The highest exergy destruction of the solar system which was around 99% occurred in the morning and at the beginning of the operation. The amount of absorbed energy at the beginning of the day was low and at the same time, heat losses were high because of low ambient temperature resulted in low exergy efficiencies. By the passage of time and increase in the amount of absorbed energy, the irreversibility of the solar system decreased. For Cases I and II, the exergy efficiency fluctuated between 4% and 5% for a noticeable amount of time from 10:30 AM to 3 PM. At the end of the operation, the exergy efficiency increased and reached 6%. The reason for this increase was that while the solar radiation was decreasing significantly, the outlet temperature of the collector and absorbed energy by the solar working fluid were still relatively high. The results also indicate that the overall trend of exergy efficiency followed the same trend in both cases. However, the system performed slightly better in Case II compared to Case I.

The application of a cooling unit in Case II resulted in lower permeate flow temperatures which entered the membrane module through the cold channel. Due to the increase in temperature difference across the membrane module and heat transfer rate, the temperature of the feed stream coming out of the membrane and returning to the feed tank decreased. The overall result was having lower saline water temperature inside the feed tank which in return decreased the collector inlet temperature. The absorbed energy by the solar working fluid increased as its temperature was lower, and higher values of absorbed energy led to higher exergy efficiencies. Overall, one can conclude that implementing any strategy that increases the difference between collector inlet and outlet temperatures results in a positive effect on the exergy efficiency of the solar system.

The exergy efficiency in Case III followed the same pattern as the other two cases by having a low value at the beginning of the day and increasing by the passage of time. However, the exergy efficiency of Case III was lower than other two cases at the beginning of the operation which can be contributed to the fact that the ambient temperature in Case III was lower especially in the morning resulted in higher thermal losses. By the passage of time, the difference between exergy efficiencies decreased, however, the exergy efficiency in Case III was still lower than the other two cases.

Table 4 provides information regarding the averaged exergy efficiency of the components of the solar system as well as its overall exergy efficiency. The highest irreversibility or exergy destruction in all cases clearly occurred in HPSC (i.e. 95.54%, 95.4%, and 96.6% in Cases I, II, and III, respectively). This is followed by heat exchanger and the circulating pump. The exergy destruction in the HPSC was approximately 3.45, 3.48, and 5.23 times higher than exergy destruction in the heat exchanger and the circulating pump for cases I, II, and III, respectively. The overall exergy efficiency in Cases I, II, and III were 5.48%, 5.68%, and 4.18%, respectively.

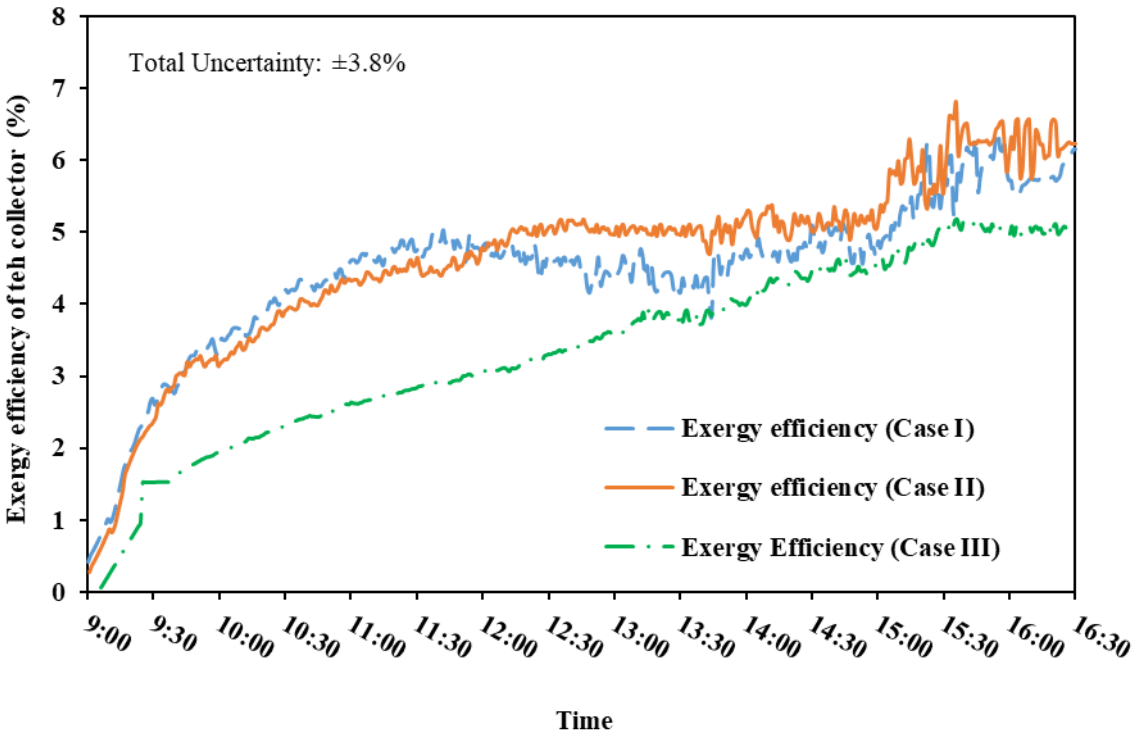

Fig. 8. Exergy efficiency of the HPSC as a function of time

Table 4. The averaged exergy efficiencies of the components of the solar heating system

Case	Collector	Pump	Heat exchanger	Overall
Case I	4.46	15.49	15.35	5.48
Case II	4.6	16.13	15.9	5.65
Case III	3.4	18.73	16.82	4.18

4.2. Membrane-based desalination system

Figure 9a shows the feed and permeate temperatures at inlet and outlet ports of the DCMD module in Case I under normal operational conditions and Case II in which the permeate flow cooling unit (PFCU) was applied. The cooling unit was arranged in a way to keep the permeate flow temperature at 30±3 °C. In addition, Fig. 9b shows the inlet temperature difference between two sides of the membrane in both Cases I and II.

At the beginning of the operation and because of low solar radiation, the solar system was not able to provide all the required energy to increase the temperature of saline water inside the feed tank. Therefore, the electric auxiliary heater was on for about 15 minutes between 9 to 9:30 AM. The auxiliary heater increased the inlet temperature difference between two sides of the membrane from 3 °C to around 18 °C. By the passage of time and the increase in solar radiation, the solar system operated independently and provided all the required thermal energy. This proved the capability of the proposed solar system to drive the desalination system throughout most of the day.

As expected, the permeate flow temperature in Case I increased by the passage of time due to continuous heat transfer in the membrane module. The permeate flow temperature reached 40 °C at around 12:30 and remained almost constant afterwards. This increase in permeate flow temperature decreases the temperature difference between two surfaces of the membrane resulting in lower mass flux through the membrane and lower overall efficiency of the system. Therefore, by having almost similar feed flow temperatures in both cases and lower permeate flow temperature in Case II, higher freshwater production was expected in Case II compared to Case I.

The inlet temperature difference between two sides of the membrane, which acts as a key parameter affecting the water productivity of the membrane, followed the same pattern. The inlet temperature difference between two sides of the membrane was almost similar before 10:30 AM. However, the permeate flow inlet temperature in Case I increased afterwards due to continuous heat transfer in the membrane module resulting in lower inlet temperature difference between two sides of the membrane compared to Case II. Considering the gap exists between the graphs of Fig. 9b and comparing the inlet temperature difference between two sides of the membrane in both cases reveal the effectiveness of applying the cooling unit in increasing the mass flux through the membrane.

In addition, the temperature of the permeate flow which comes from the feed storage tank is slightly lower in Case II than Case I. This confirms the results presented in Fig. 7 stating that the application of PFCU results in having lower temperatures of feed stream coming out of the membrane and returning to the feed tank which in return decreases the average temperature of saline water inside the feed tank.

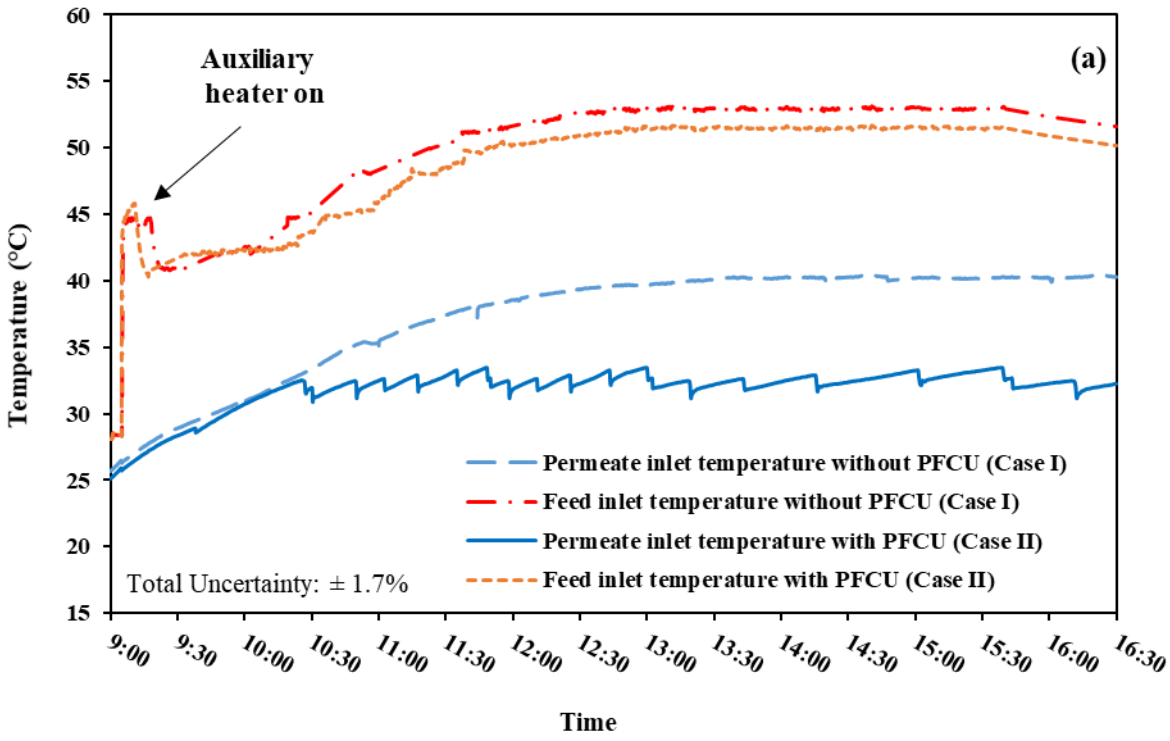

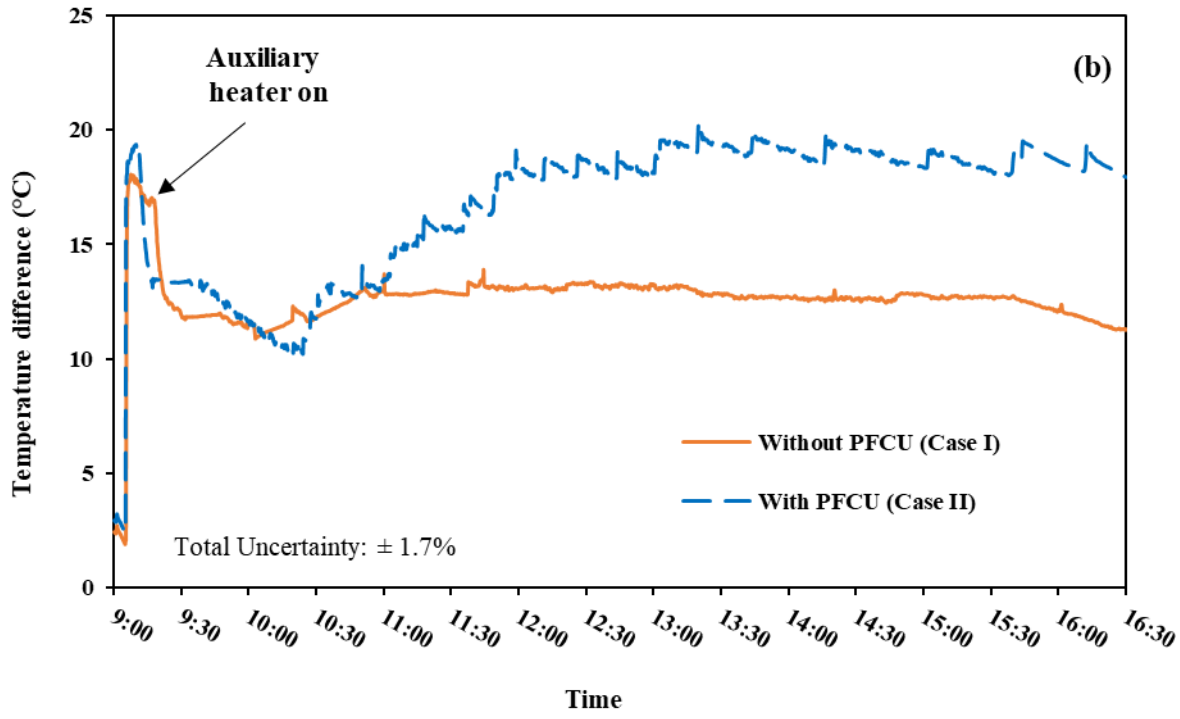

Fig. 9. (a) Feed and permeate temperatures at inlet and outlet ports of the DCMD module in Cases I and II, and (b) Inlet temperature difference between two sides of the membrane

Figure 10 depicts the hourly average freshwater production rate of the system under operational conditions of Cases I, II, and III. The overall trend of hourly average freshwater production rate is ascending in both Cases I and II. The reason for this trend is the increase in temperature difference between the two surfaces of the membrane. The freshwater production rates in Cases I and II at 10 AM are 1.88 and 2.58 L/m^{2}h, respectively. This parameter reached the high values of 2.65 and 3.64 L/m^{2}h and maximum values of 2.78 and 3.81 L/m^{2}h for Cases I and II, respectively. In addition, the hourly average freshwater production rate in Case II was higher than Case I at all times. This is chiefly because of the positive effect of implementing the PFCU on the performance of DCMD module resulting in higher mass flux through the membrane. For instance, the system in Case II had 37.2%, 37.6%, and 37% higher freshwater production rates at 10 AM, 13 PM, and 16 PM, respectively.

However, the overall trend of the hourly average freshwater production rate in Case III was different from the other two cases. The freshwater production rate was ascending until 2 PM and started to decrease afterwards. The main reason for this behaviour is the fact that the day was shorter in winter and the solar radiation intensity dropped significantly in the afternoon. Consequently, the outlet temperature of the collector and the inlet feed temperature of the DCMD module decreased resulted in lower mass flux through the membrane.

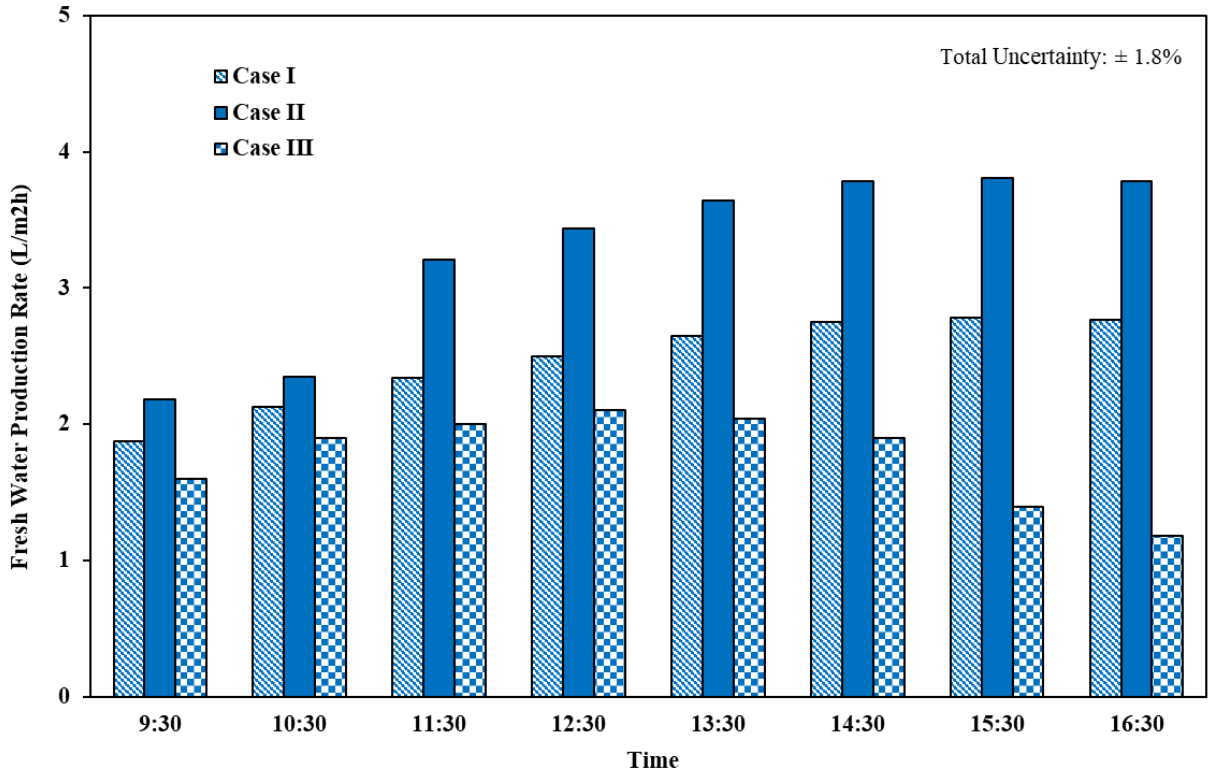

Fig. 10. Hourly average freshwater production rate of the solar desalination system

4.3. Gained output ratio

Figure 11 indicates the hourly average values of gained output ratio (GOR) of the desalination system under operational conditions of Cases I (without PFCU) and II (with PFCU). The GOR in both cases has an ascending trend starting from 0.32 and 0.39 for Cases I and II, respectively, and reaching the maximum values of 0.77 and 0.87 at around 14 PM. This is mainly because of the increase in temperature difference and consequently in the vapour pressure difference

between the two sides of the membrane module. The results show a slight decrease in GOR values after 16 PM which was due to a decrease in solar radiation and its consequent effect on having lower feed tank temperature. As a result, the feed flow entered the membrane at lower temperatures and reduced the mass flux through the membrane.

Another visible feature of this figure is the improvement in GOR values upon implementing the PFCU in the permeate flow loop. For instance, the GOR values in Cases I and II were respectively 0.4 and 0.44 at 11 AM which show a GOR improvement of 10%. The GOR improvement reached 14.5% and 7.5% at 15 PM and 16 PM, respectively. Overall, the results prove the technical effectiveness of implementing a PFCU in the permeate flow loop on the performance improvement of the desalination system.

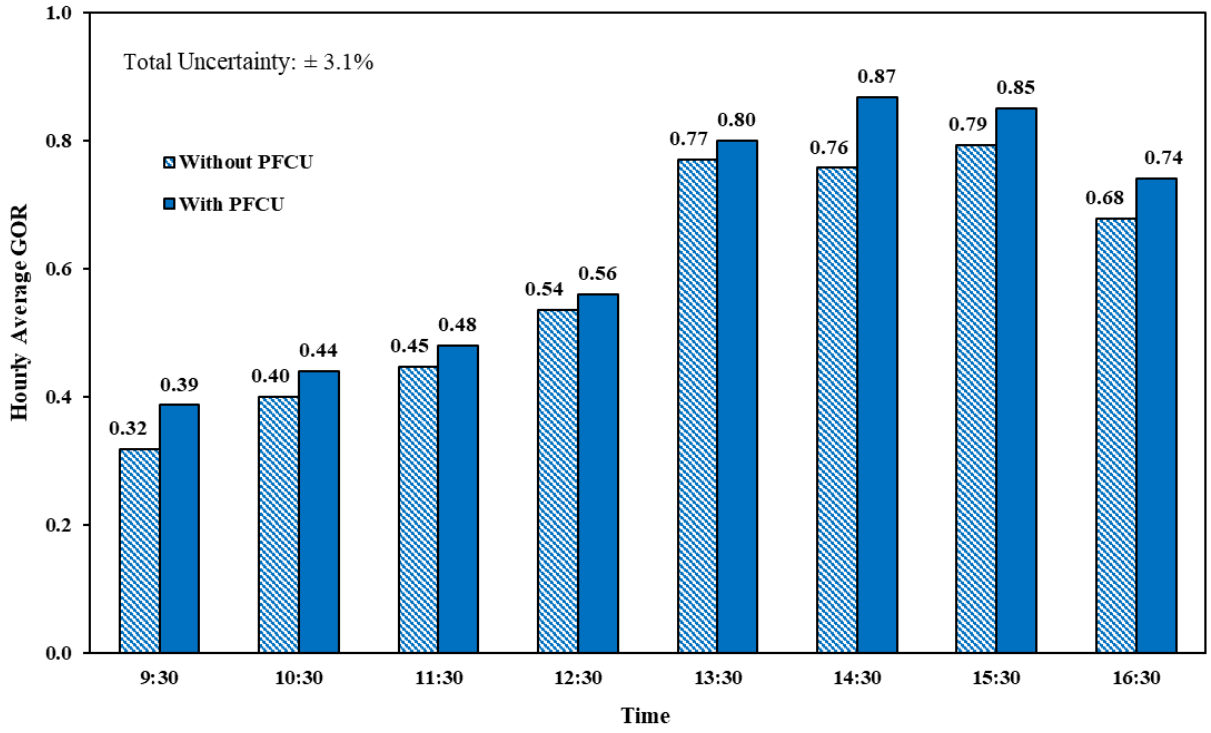

Fig. 11. Hourly average values of gained output ratio of the desalination system under operational conditions of Cases I and II

4.4. Overall efficiency of solar membrane-based desalination system

Figure 12 shows the hourly averaged overall efficiency of the solar driven membrane-based desalination system (Eq. 11) under operational conditions of Cases I, II, and III. The overall efficiency almost followed the same trend in all cases. The overall efficiency was low at the beginning of the operation due to low values of freshwater production rate. By the passage of time, the solar radiation, feed tank temperature and at the same time freshwater production rate increased. As a result, both the nominator and denominator of Eq. (11) increased resulting in hourly average efficiencies in the ranges of 19.3-21.3%, 26.9-29.6%, and 11.8-13.2% for Cases I, II, and III, respectively. By moving towards the afternoon, the solar radiation started to slightly decrease, however, the feed tank temperature was still high leading to higher average efficiencies. The average efficiency of the solar desalination system reached 36.9-46.6%, 49.4-61.8%, and 34.6-39.3% in Cases I, II, and III, respectively, at the last final hours of the operation.

Moreover, the results indicate the advantage of using a PFCU in the permeate loop of the solar desalination system at all times. The average efficiencies of the system in case II were 36% and 36.7% higher than Case I at 12 PM and 13 PM, respectively. In addition, the overall efficiency improvement was around 33% at 16 PM. Overall, these data support the technical effectiveness of implementing a PFCU in the permeate flow loop of the system.

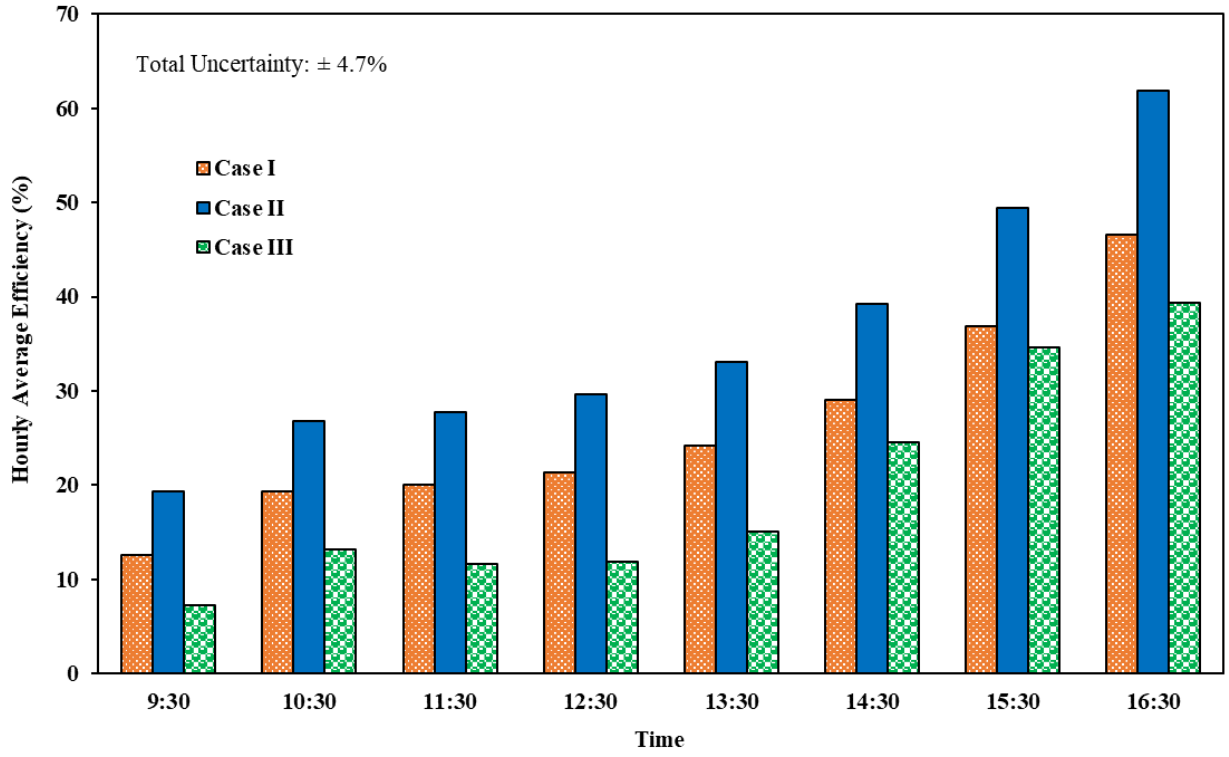

Fig. 12. Hourly averaged overall efficiency of the solar driven membrane-based desalination system

4.5. Specific energy consumption

Figure 13 depicts the hourly averaged specific energy consumption of the proposed solar driven membrane-based desalination system. The system had its highest specific energy consumption (i.e. around 1000 kWh/m^3) at the beginning of the operation which was mainly due to the application of auxiliary electric heater. In addition, the feed temperature and consequently the mass flux through the membrane were relatively low. Afterwards, the specific energy consumption decreased and reached the minimum values of 250 and 236 kWh/m^3 at 14:30 in Cases I and II, respectively, and the minimum value of 304 kWh/m^3 at 12:30 in Case III.

It is interesting to notice that the specific energy consumption remained low in the afternoon in Cases I and II while it had an increasing trend after 14:30 in Case III. The main reason for this difference was that in winter the days were shorter resulted in lower values of solar

radiation, feed temperature, and consequently fresh water production. Meanwhile, the solar radiation and water production in summer were relatively high until 16:30. The daily averaged specific energy consumption in winter was higher than summer with quantitative values of 407, 377, and 450 kWh/m^3 in Cases I, II, and III, respectively.

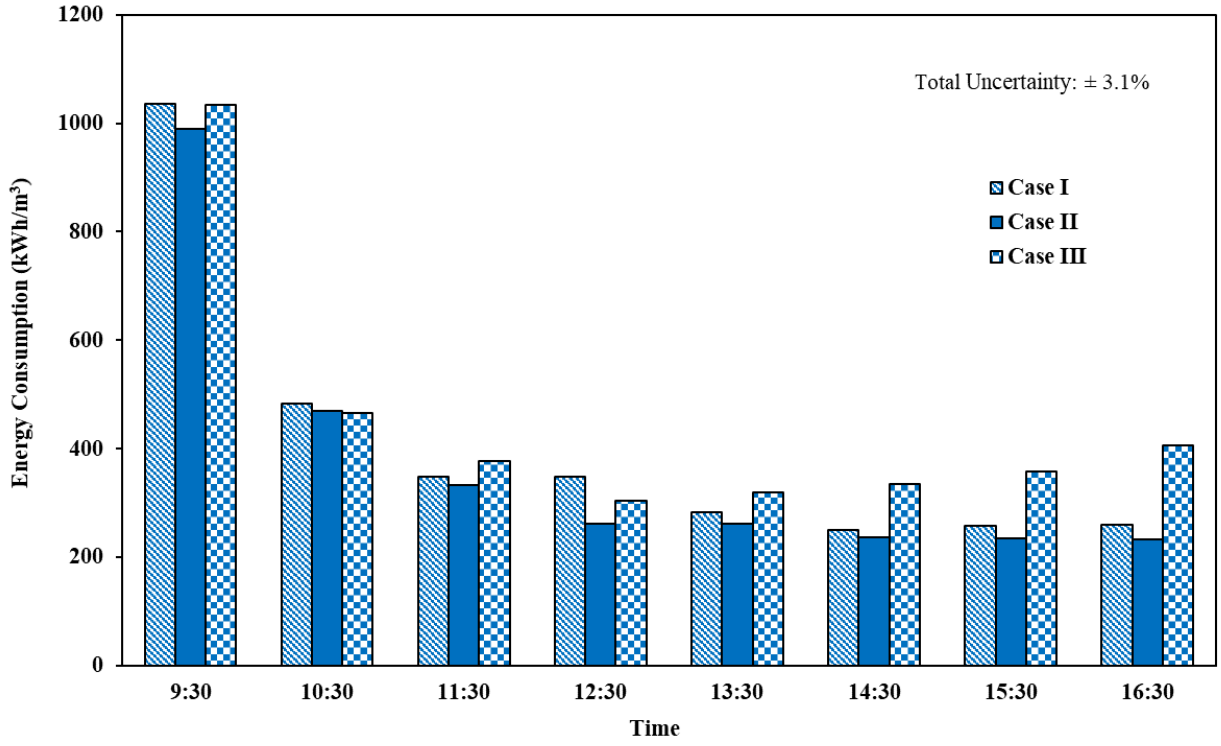

Fig. 13. Hourly averaged specific energy consumption variations in different cases.

4.6. Economic analysis

Economic analysis in this study was principally based on the analysis of the capital cost, operational energy consumption, saved energy, and payback period. Capital cost comprised the cost of materials, equipment, and installation, while the operating energy consumption included the electricity bill. To determine the payback period and by considering the inflation rates, the overall value of saved water and energy costs minus operating cost was calculated for each year. These values were added up to reach the capital cost of the system.

The three pumps had the overall power consumption of 138 W, and considering the 7.5 hours of operation, consumed around 1 kWh in a day. The heater had the power consumption of 3 kW and was operated for around 15 minutes in the morning. It is worth noting that the price of electricity and water in Australia are approximately 0.54 AUD/kWh and 0.25 AUD/L, respectively. the results showed that the payback period of the system is around 2.7 years. The equipment, operating, and total costs are presented in Table 5.

Table 5. equipment, operating, and capital, and saved costs of the system

Item	**Price (AUD)**
HPSC	700
DCMD module	975
Pumps	570
Storage tanks	650
Power and control unit	750
Piping and connections	450
Installation	500
Expansion tank	350
Capital cost	**4,950**
Pumps operation cost	200
Electric heater operation cost	150
Annual operation cost	**350**
Annual saved water cost	**1,825**

5. Conclusions

This paper experimentally investigated the performance of a novel integrated heat pipe solar-driven membrane-based desalination system under real climatic conditions of Perth, Western Australia in summer (Case I) and winter (Case III) without implementing the cooling unit. The technical effectiveness of adding the cooling unit to the permeate loop of the desalination system on freshwater production rate, gained output ratio, and overall efficiency of the system was studied in Case II. The following results were obtained:

- The heat pipe solar system was able to operate independently and provided all the required thermal energy of the desalination system except 15 minutes in the morning.
- The maximum thermal efficiency of the solar system in summer days reached ~78% while its exergy efficiency fluctuated between 4% and 5% for a noticeable amount of time. The exergy efficiency in winter days had an ascending trend reaching its maximum value of ~5% at the end of the day.
- The freshwater production rate in summer days reached 2.65 and 3.64 L/m^2h at 14 PM for the system without and with the cooling unit, respectively. The maximum values of the mentioned parameters were 2.78 and 3.81 L/m^2h, respectively. The freshwater production rate in winter days had a parabolic trend reaching its maximum value of 2.1 L/m^2h at around 12:30 PM.
- The gained output ratio and overall efficiency of the system were shown to be improved upon application of a cooling unit in the permeate flow loop of the system indicating the effectiveness of the proposed configuration. However, the economic feasibility of implementing the cooling unit needs further investigations.
- The hourly averaged overall efficiency almost had similar pattern in all cases, however, Case II had the highest and Case III had the lowest values throughout the day.

- The system had higher daily averaged specific energy consumption in winter compared to summer with quantitative values 407, 377, and 450 kWh/m^3 in Cases I, II, and III, respectively.

Optimizing the solar system considering physical parameters (e.g., number of heat pipes), as well as operational parameters (e.g., solar working fluid mass flow rate), has great research potential. A theoretical study to find the optimum characteristics of the membrane-based desalination system is also recommended as a research direction. In addition, modeling-based analysis or estimation of system annual output and economic viability have a significant research potential.

Acknowledgments

The authors would like to express their gratitude to Dr Alireza Mohyeddin for his kind assistance during the experimental phase of this project.

References

[1] M.R. Qtaishat, F. Banat. Desalination by solar powered membrane distillation systems. Desalination. 308 (2013) 186-97.
[2] K. Nakoa, K. Rahaoui, A. Date, A. Akbarzadeh. Sustainable zero liquid discharge desalination (SZLDD). Solar Energy. 135 (2016) 337-47.
[3] J.P. Holman. Experimental Methods for Engineers. 8th ed. McGraw-Hill2011.
[4] https://www.watercorporation.com.au.
[5] S.J. Mamouri, H.G. Derami, M. Ghiasi, M. Shafii, Z. Shiee. Experimental investigation of the effect of using thermosyphon heat pipes and vacuum glass on the performance of solar still. Energy. 75 (2014) 501-7.
[6] V. Eveloy, P. Rodgers, L. Qiu. Hybrid gas turbine-organic Rankine cycle for seawater desalination by reverse osmosis in a hydrocarbon production facility. Energy Convers Manage. 106 (2015) 1134-48.

[7] W.F. He, D. Han, C. Yue, W.H. Pu. A parametric study of a humidification dehumidification (HDH) desalination system using low grade heat sources. Energy Convers Manage. 105 (2015) 929-37.
[8] B. Ghorbani, M. Mehrpooya, M. Sadeghzadeh. Developing a tri-generation system of power, heating, and freshwater (for an industrial town) by using solar flat plate collectors, multi-stage desalination unit, and Kalina power generation cycle. Energy conversion and management. 165 (2018) 113-26.
[9] R. Miladi, N. Frikha, A. Kheiri, S. Gabsi. Energetic performance analysis of seawater desalination with a solar membrane distillation. Energy conversion and management. 185 (2019) 143-54.
[10] A.M. Elzahaby, A.E. Kabeel, M.M. Bassuoni, A.R.A. Elbar. Direct contact membrane water distillation assisted with solar energy. Energy Convers Manage. 110 (2016) 397-406.
[11] G. Zuo, R. Wang, R. Field, A.G. Fane. Energy efficiency evaluation and economic analyses of direct contact membrane distillation system using Aspen Plus. Desalination. 283 (2011) 237-44.
[12] D. González, J. Amigo, F. Suárez. Membrane distillation: Perspectives for sustainable and improved desalination. Renewable and Sustainable Energy Reviews. 80 (2017) 238-59.
[13] M. Khayet. Solar desalination by membrane distillation: Dispersion in energy consumption analysis and water production costs (a review). Desalination. 308 (2013) 89-101.
[14] A. Shafieian, M. Khiadani, A. Nosrati. Performance analysis of a thermal-driven tubular direct contact membrane distillation system. Applied Thermal Engineering. (2019) 113887.
[15] S. T.Bouguecha, S. E.Aly, M. H.Al-Beirutty, M. M.Hamdi, A. Boubakri. Solar driven DCMD: Performance evaluation and thermal energy efficiency. Chemical Engineering Research and Design. 100 (2015) 331-40.
[16] W.G. Shim, K. He, S. Gray, I.S. Moon. Solar energy assisted direct contact membrane distillation (DCMD) process for seawater desalination. Sep Purif Technol. 143 (2015) 94-104.
[17] Q. Ma, A. Ahmadi, C. Cabassud. Direct integration of a vacuum membrane distillation module within a solar collector for small-scale units adapted to seawater desalination in remote places: Design, modeling & evaluation of a flat-plate equipment. J Membrane Sci. 564 (2018) 617-33.
[18] M.A. Sabiha, R. Saidur, S. Mekhilef, O. Mahiand. Progress and latest developments of evacuated tube solar collectors. Renew Susta Energy Rev. 51 (2015) 1038-54.
[19] A.E. Kabeel, M. Abdelgaied, E.M.S. El-Said. Study of a solar-driven membrane distillation system: Evaporative cooling effect on performance enhancement. Renew Energy. 106 (2017) 192-200.
[20] A. Chafidz, S. Al-Zahrani, M.N. Al-Otaibi, C.F. Hoong, T.F. Lai, M. Prabu. Portable and integrated solar-driven desalination system using membrane distillation for arid remote areas in Saudi Arabia. Desalination. 345 (2014) 36-49.
[21] F. Suárez, J.A. Ruskowitz, S.W. Tyler, A.E. Childressd. Renewable water: Direct contact membrane distillation coupled with solar ponds. Appl Energy. 158 (2015) 532-9.
[22] K. Rahaoui, L.C. Ding, L.P. Tan, W. Mediouri, F. Mahmoudi, K. Nakoa, et al. Sustainable Membrane Distillation Coupled with Solar Pond. Energy Proc. 110 (2017) 414-9.
[23] Y.-D. Kim, KyawThu, N. Ghaffour, K.C. Ng. Performance investigation of a solar-assisted direct contact membrane distillation system. J Membrane Sci. 427 (2013) 345-64.
[24] H. Chang, S.-G. Lyu, C.-M. Tsai, Y.-H. Chen, T.-W. Cheng, Y.-H. Chou. Experimental and simulation study of a solar thermal driven membrane distillation desalination process. Desalination. 286 (2012) 400-11.

[25] J. Koschikowski, M. Wieghaus, M. Rommel. Solar thermal-driven desalination plants based on membrane distillation. Desalination. 156 (2003) 295-304.
[26] H.K. Palanisami Nallasamy, Moon Shik. . Utilization of solar energy for direct contact membrane distillation process: an experimental study for desalination of real seawate. Korean J Cheml Eng. 31 (2014) 155-61.
[27] S.R. Selvi, R. Baskaran. Desalination of well water by solar power membrane distillation and reverse osmosis and its efficiency analysis. Int J ChemTech Research. 6 (2014) 2628-36.
[28] M.R. Qtaishat, F. Banat. Desalination by solar powered membrane distillation systems. Desalination. 308 (2013) 186-97.
[29] H. Sharon, K.S. Reddy. A review of solar energy driven desalination, technologies. Renew Sust Energy Rev. 41 (2015) 1080-118.
[30] A. Shafieian, M. Khiadani, A. Nosrati. A review of latest developments, progress, and applications of heat pipe solar collectors. Renew Sust Energy Rev. 95 (2018) 273-304.
[31] A. Shafieian, M. Khiadani, A. Nosrati. Strategies to improve the thermal performance of heat pipe solar collectors in solar systems: A review. Energy Convers Manage. 183 (2019) 307-31.
[32] B. Rassamakin, S. Khairnasov, V. Zaripov, A. Rassamakin, O. Alforova. Aluminum heat pipes applied in solar collectors. Sol Energy. 94 (2013) 145-54.
[33] D. Mangal, D. Lamba, T. Gupta, K. Jhamb. Acknowledgement of evacuated tube solar water heater over flat plate solar water heater. Int J Eng. 4 (2010) 279-84.
[34] A. Shafieian, M. Khiadani, A. Nosrati. Thermal performance of an evacuated tube heat pipe solar water heating system in cold season. Appl Therm Eng. 149 (2019) 644-57.
[35] Century Sun Energy Technology. Shanghai, China. http://www.shcenturysun.com/productlistshow_6.html.
[36] A. Shafieian, J.J. Osman, M. Khiadani, A. Nosrati. Enhancing heat pipe solar water heating systems performance using a novel variable mass flow rate technique and different solar working fluids. Solar Energy. 186 (2019) 191-203.
[37] MICRODYN NADIR. Germany. https://www.microdyn-nadir.com/tubular-capillary-modules.
[38] E. Azad. Theoretical and experimental investigation of heat pipe solar collector. Exp Therm Fluid Sci. 32 (2008) 1666-72.
[39] R. Daghigh, A. Shafieian. An experimental study of a heat pipe evacuated tube solar dryer with heat recovery system. Renewable energy. 96 (2016) 872-80.
[40] H. Gunerhan, A. Hepbasli. Exergetic modeling and performance evaluation of solar water heating systems for building applications. Energy Build. 39 (2007) 509-16.
[41] E.K. Akpinar, F. Koçyiğit. Energy and exergy analysis of a new flat-plate solar air heater having different obstacles on absorber plates. Appl Energy. 87 (2010) 3438-50.
[42] R. Daghigh, A. Shafieian. Energy-exergy analysis of a multipurpose evacuated tube heat pipe solar water heating-drying system. Experimental Thermal and Fluid Science. 78 (2016) 266-77.
[43] R. Daghigh, A. Shafieian. Theoretical and experimental analysis of thermal performance of a solar water heating system with evacuated tube heat pipe collector. Applied Thermal Engineering. 103 (2016) 1219-27.
[44] R. Daghigh, A. Shafieian. Energy and exergy evaluation of an integrated solar heat pipe wall system for space heating. Sādhanā. 41 (2016) 877-86.
[45] I. Dincer, M.A. Rosen. Exergy: energy, environment and sustainable development. Newnes2012.
[46] R.J. Moffat. Describing the uncertainties in experimental results. Exp Ther Fluid Sci. (1988) 3-17.